

LA-UR-15-25295 (Accepted Manuscript)

## High pressure and temperature equation of state and spectroscopic study of CeO

Jacobsen, Matthew  
Velisavljevic, Nenad  
Dattelbaum, Dana McGraw  
Chellappa, Raja Shankar

Provided by the author(s) and the Los Alamos National Laboratory (2016-06-29).

**To be published in:** Journal of Physics: Condensed Matter

**DOI to publisher's version:** 10.1088/0953-8984/28/15/155401

**Permalink to record:** <http://permalink.lanl.gov/object/view?what=info:lanl-repo/lareport/LA-UR-15-25295>

**Disclaimer:**

Approved for public release. Los Alamos National Laboratory, an affirmative action/equal opportunity employer, is operated by the Los Alamos National Security, LLC for the National Nuclear Security Administration of the U.S. Department of Energy under contract DE-AC52-06NA25396. Los Alamos National Laboratory strongly supports academic freedom and a researcher's right to publish; as an institution, however, the Laboratory does not endorse the viewpoint of a publication or guarantee its technical correctness.

## High pressure and temperature equation of state and spectroscopic study of $\text{CeO}_2$

This content has been downloaded from IOPscience. Please scroll down to see the full text.

2016 J. Phys.: Condens. Matter 28 155401

(<http://iopscience.iop.org/0953-8984/28/15/155401>)

View [the table of contents for this issue](#), or go to the [journal homepage](#) for more

Download details:

IP Address: 192.12.184.7

This content was downloaded on 28/03/2016 at 13:48

Please note that [terms and conditions apply](#).

# High pressure and temperature equation of state and spectroscopic study of CeO<sub>2</sub>

M K Jacobsen<sup>1</sup>, N Velisavljevic<sup>1</sup>, D M Dattelbaum<sup>1</sup>, R S Chellappa<sup>2</sup>  
and C Park<sup>3</sup>

<sup>1</sup> Shock and Detonation Physics (M-9), PO Box 1663, MS P952, Los Alamos National Laboratory,  
Los Alamos, NM 87545, USA

<sup>2</sup> Materials Science and Technology (MST-8), PO Box 1663, MS H805, Los Alamos National Laboratory,  
Los Alamos, NM 87545, USA

<sup>3</sup> HPCAT, Geophysical Laboratory, Carnegie Institution of Washington, 9700 S. Cass Ave., Bldg. 434E,  
Argonne, IL 60439, USA

E-mail: [mjacobson@lanl.gov](mailto:mjacobsen@lanl.gov)

Received 25 January 2016, revised 23 February 2016

Accepted for publication 24 February 2016

Published 17 March 2016



## Abstract

One of the most widely used x-ray standards and a highly applied component of catalysis systems, CeO<sub>2</sub> has been studied for the purpose of better understanding its equation of state and electronic properties. Diamond anvil cells have been used to extend the equation of state for this material to 130 GPa and explore the electronic behavior with applied load. From the x-ray diffraction studies, it has been determined that the high pressure phase transition extends from approximately 35–75 GPa at ambient temperature. Elevation of temperature is found to decrease the initiation pressure for this transition, with multiple distinct temperature regions which indicate structural related anomalies. In addition, hydrostatic and non-hydrostatic effects are compared and exhibit a drastic difference in bulk moduli. The electronic results indicate a change in the scattering environment of the cerium atom, associated with the high pressure phase transition. Overall, these results present the first megabar pressure study and the first high pressure and temperature study of ceria. Additionally, this shows the first combined study of the *K* and *L*<sub>III</sub> edges of this material to 33 GPa.

Keywords: ceria, high pressure, equation of state, spectroscopy

(Some figures may appear in colour only in the online journal)

## 1. Introduction

Ceria, or cerium dioxide (CeO<sub>2</sub>), has recently attracted a diverse range of attention due to highly interesting technical applications, such as solid oxide fuel cells [1, 2], catalysts [1, 3], optical components [4, 5], and potential microelectronic applications [6]. Under ambient conditions, ceria crystallizes in the fluorite structure (Fm3m, space group 225). Pressures around 30 gigapascals (GPa) have been found to cause a transformation to space group 62, as demonstrated by x-ray diffraction (XRD) [7, 8] and Raman studies [9]. For the

high pressure phase, work by Duclos [7] reports a *Pnam* space group and Liu [10] reports *Pbnm*.

Beyond this, information about the compressibility and electronic properties are not widely available and are essential for construction of an accurate equation of state (EOS). While compressibility has been probed, measurements are limited in pressure to 70 GPa and show varying effects of hydrostaticity. For example, it is known that a hydrostatic environment can alter the transition pressure or bulk modulus when compared with a similar non-hydrostatic environment [11, 12]. Reports on the bulk modulus for theoretical and experimental studies, compiled in Gerward *et al* [8], span the range from 176 to 357 GPa, which more sharply illustrates how important the hydrostatic environment can be. The added influence of temperature can also have strong effects on the crystal structure.



Original content from this work may be used under the terms of the [Creative Commons Attribution 3.0 licence](https://creativecommons.org/licenses/by/3.0/). Any further distribution of this work must maintain attribution to the author(s) and the title of the work, journal citation and DOI.

Yashima *et al*'s work [13] is an excellent example, where they used neutron diffraction to study O structural disorder and showed elevated temperatures result in the O ions bulging along the body center and *c*-axis of the crystal.

It is also unclear what effect pressure has on the electronic properties of CeO<sub>2</sub>, as no investigations of this sort were found. In contrast, valence effects induced by ion beam exposure [14] have been found to increase the trivalent character of the compound at ambient pressure. Ultimately, more information about the high pressure crystalline or electronic structure is needed to better understand both and enhance usage in applications. To remedy this lack of information, this work presents high pressure spectroscopic and high temperature/pressure equation of state results for CeO<sub>2</sub>.

## 2. Experimental details and data analysis

All experiments described involved ceria powder of 99.5% purity (325 mesh, American Elements). High pressure EOS experiments were undertaken at Sector 16 of the advanced photon source (APS), using beamlines 16-ID-B and 16-BM-D ( $\lambda = 0.406\,626$  and  $0.424\,603$  Å, respectively). Samples were co-loaded with ruby [15] and Pt [16] for pressure calibration with either neon for pressure transmission or no pressure medium. Ruby was used during the gas loading process to determine the starting pressure and success of the gas loading attempt. For high temperature measurements, gas loaded cells were placed in a recently developed vacuum furnace (max  $T \approx 400$  °C) at the 16-BM-D beamline. Pressure on all cells was controlled using a remote gas membrane setup and isothermal compression curves were collected at 100 °C increments up to 300 °C using a MAR image plate.

All resulting patterns were integrated using Fit2D [17] and Rietveld refinement was performed on the ambient phase and pressure standard using MDI's JADE [18] with the high pressure phase refined as a structureless (i.e. no atoms) phase. In these fits, a Pearson-VII peak shape was used with the full-width at half-maximum refined individually for each peak. Results from these fits displayed Rp values less than 5% for the refinement and determinations of the platinum unit cell parameter was used to determine pressure errors, amounting to approximately 1% of the applied pressure. An example fit for the high pressure phase is shown in figure 3(b). EOS data was obtained using the EOSfit GUI software [17] using a third-order Birch–Murnaghan fit. Data and standard errors for each were included in the fit results, with all parameters fit simultaneously.

In addition, CeO<sub>2</sub> was loaded in a Be gasket with a 125  $\mu\text{m}$  hole between 300  $\mu\text{m}$  anvils to investigate the electronic structure with pressure. Ruby was used as an internal calibrant [15], with pressure determined from the average pressure across the sample chamber. Resonant inelastic x-ray scattering (RIXS), at beamline 16-ID-D at the APS [19], was used with the incident energy set at the cerium  $L_{\text{III}}$  edge (5.723 keV). The signal was analyzed by a spherically-bent Si crystal and an AmpTek detector in a Rowland circle. A similar setup was used to perform the lower pressure x-ray diffraction (hydrostatic/neon and non-hydrostatic/no medium)

and x-ray absorption near edge spectroscopy (XANES) using the cerium  $K$  edge (40.443 keV) at beamline 16-BM-D at the APS. Specific details of the technique are presented elsewhere [20]. 300  $\mu\text{m}$  culet diamonds were used with a spring steel gasket, pre-indented to 50  $\mu\text{m}$  thick and a 150  $\mu\text{m}$  hole and samples were co-loaded with the same calibrants used for the 130 GPa experiment. XANES measurements were performed using pre- and post-sample ion chambers to normalize data *in situ*. For both spectroscopy (RIXS and XANES) experiments, the energy resolution is approximately 1 eV, with four patterns collected at each pressure and averaged to reduce measurement noise.

## 3. Results and discussion

### 3.1. High temperature and pressure diffraction results

Refinement results for the high pressure, ambient temperature XRD unit cell volume (Å<sup>3</sup>) versus pressure data are shown in figure 1. Evolution of the unit cell parameters for the high pressure phase have also been evaluated and show the *c*-axis is much stiffer than the remaining two, as shown in figure 2. The previously reported transition was found to begin around 35.6 GPa and remained to 73 GPa in hydrostatic loading. Co-existence of the two phases is clearly seen in the XRD patterns shown in figure 3. From our study, the best fit for the high pressure phase was obtained with the *Pnam* space group and unit cell parameters at 73.5 GPa of  $a = 5.535(2)$ ,  $b = 6.478(2)$ , and  $c = 3.363(1)$ . Further, the compression of the orthorhombic phase has been found to result in isotropic compression, as the trend for each lattice constant is. It is immediately seen that there are significant differences between the hydrostatic and non-hydrostatic experiments. Non-hydrostatic samples show a much higher bulk modulus ( $B_0$ ) than the hydrostatic counterpart, as shown in table 1. Non-hydrostatic loading was found to initiate the high pressure transition approximately 5 GPa lower than the hydrostatic environment. Similar behavior has been previously seen for several other rare-earth bearing oxide materials, as reported by Errandonea *et al* [21].

As can be seen from these results, the equation of state parameters compare favorably with previously reported values. This transition results in a  $7.6 \pm 0.2\%$  volume collapse, comparing favorably with the  $7.5 \pm 0.7\%$  reported by Duclos [7] and  $9.8\%$  reported by Gerward [23]. Although the results in table 1 indicate Gerward's [23] work as being hydrostatic, the pressure medium used was 4:1 methanol:ethanol which is known to become non-hydrostatic above 10 GPa [24, 25]. As a result, data above 10 GPa using methanol:ethanol media can be expected to align better with non-hydrostatic data, as is seen in the equation of state plots (figure 1).

The high temperature isotherms show increasing temperature leads to an earlier initiation to the phase transition, evidenced in the equation of state data in figure 4(a). The transformation is found to begin around 28 GPa at 200 °C and 26 at 300 °C. Inspecting the boundary on a high pressure–temperature phase diagram, there appears similar behavior to that of zirconium [26] where high pressure

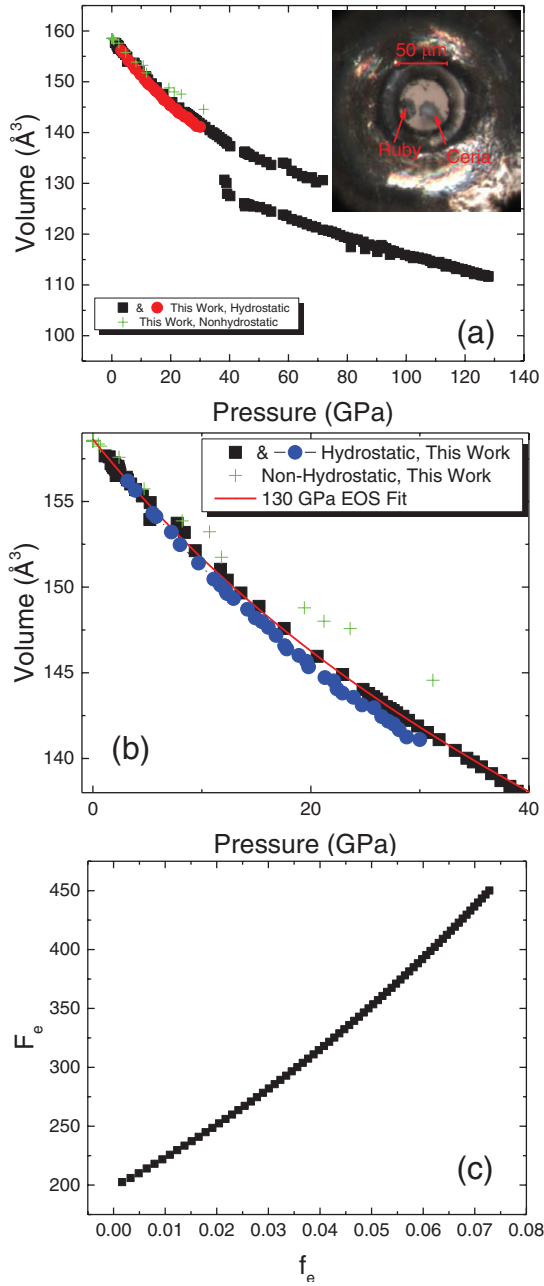


**Figure 1.** Ambient temperature unit cell volumes ( $\text{\AA}^3$ ) versus pressure obtained by angle dispersive XRD are shown (a) with an example image of the gas loading for the 130 GPa experiment. In this inset, ruby and sample are labeled with an example scale bar. In addition, a close-up region up to 40 GPa is shown (b) with the equation of state fit for the 130 GPa experiment. Errors from this work are smaller than the size of the symbol. As a check for the equation of state used, the lower panel (c) shows the  $f$ - $F$  plot for the 130 GPa experiment, demonstrating that a third-order Birch-Murnaghan fit is appropriate for this data.

and temperature induce a kink in the  $\alpha$ - $\omega$  phase boundary. While more work needs to be done to characterize this boundary, this feature appears at the initiation of the phase transformation between ambient and 200 °C, as shown in figure 4(b).

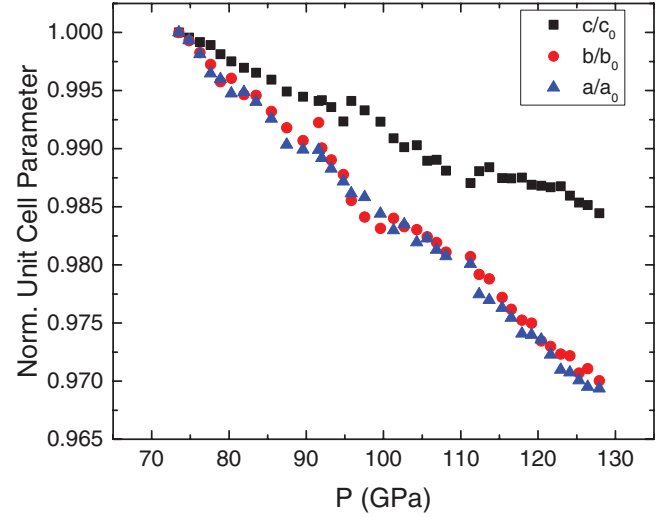


**Figure 2.** Ambient temperature normalized unit cell parameters ( $\text{\AA}$ ) versus pressure obtained by angle dispersive XRD show the  $c$ -axis being more stiff than the remaining two axes. For this plot, the unit cell values were normalized to the value at the completion of the phase transformation ( $\approx 70$  GPa).

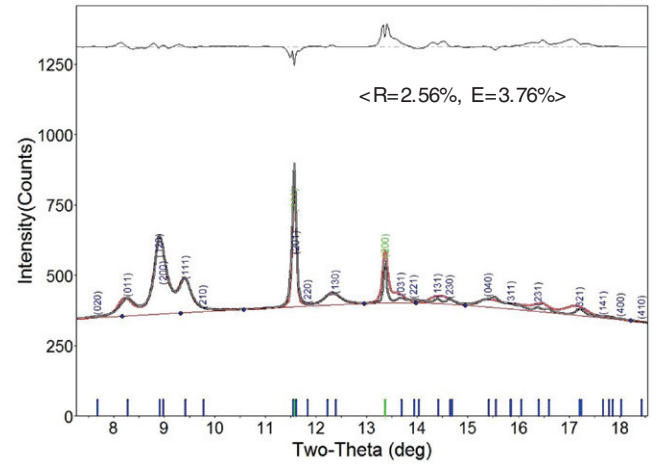


**Figure 3.** This example refinement shows the measured data (black) and the simulated pattern (red). Residuals are shown along the top of the plot and line markers are shown along the bottom (blue for  $\text{CeO}_2$  high pressure phase, green for Pt phase). HKL indices follow the same color scheme and are listed over the pattern.

### 3.2. Spectroscopic results

For the RIXS experiments, collected patterns are shown in figure 5(a). The nearly ambient pattern was found to compare very well with previous RIXS data on the ambient pressure material [27, 28]. These patterns were found to exhibit five clearly identifiable peaks, with a edge energy shift of approximately 0.8 eV over the measured pressure range. This shift did not begin until approximately 26 GPa, indicating the shift is associated with the phase transition instead of a gradual process and is in agreement with previous work to 20 GPa [27].

A similar situation is found from the results of the XANES experiments. As shown in figure 5(b), there is a clear shift

**Table 1.** Experimentally determined equation of state parameters for CeO<sub>2</sub> phases.

Temperature (°C)	P (GPa)	$V_0$ (Å <sup>3</sup> )	$B_0$ (GPa)	$B'_0$
20	130	158.63(7)	198(4)	5.4(3)
20	30	158.43(1)	188(5)	5.1(2)
20 (Non-hydro)	31	158.43(5)	262(4)	5.8(6)
100	24	158.73(6)	204(2)	4.2(2)
200	44	158.99(4)	202(3)	5.3(3)
300	43	159.80(3)	183(1)	5.4(2)
20	130	143.7(1)	287(1)	4.2(1)
20 (Non-Hydro, Ambient) [7]	70	157.9 (5)	230 (10)	4 (fixed)
20 (Non-Hydro, High P) [7]	70	121.9 (NR)	304 (25)	4 (fixed)
20 (Non-Hydro, Ambient) [10]	30	159.3 (NR)	248 (NR)	4.56 (NR)
20 (Hydro, Ambient) [23]	55	158.4 (2)	236(4)	4.4 (4)

Note: Birch–Murnaghan third-order equation of state [22] was used with all ( $V_0$ ,  $B_0$  and  $B'_0$ ) values fit using EOSFit software [17]. Estimated errors are shown in parentheses after the value. Reference values from Gerward [23], Duclos [7], and Liu [10] are included for reference below the double line. NR stands for not reported.

in the edge energy with applied load. In this, the measured XANES pattern for the ambient material is compared with that obtained at 32 GPa. The edge energy is found to shift by  $\approx 6$  eV over this pressure range. In the RIXS plot, the first post edge peak has been previously assigned as  $4f^0(\text{Ce}^{+4})$ , while the edge peak is most often assigned as  $4f^1(\text{Ce}^{+3})$  [27, 29–32]. Additionally, the pre-edge feature has been associated with  $4f$ – $4f$  interactions [33, 34]. Therefore, the shift in both these results can possibly indicate a valence shift towards a more tetravalent state. Alternately, a change in the band structure of the material could also explain the pressure induced shift. One method to investigate this is to process the RIXS data through the Demeter package (Artemis and Athena) [35]. From this, we can obtain the scattered intensity as a function of radial distance from a central cerium atom, as shown in figure 6.

From the Fourier transform and IFEFFIT calculations, both patterns show a substantial contribution from the shortest pathway (first oxygen shell). However, the ambient pattern shows a more substantial component from the next two (double scattering from first shell oxygen and single scattering from first shell cerium). In contrast, the 33 GPa pattern shows a increased contribution from the various pathways of length greater than 4 Å. Further analysis is difficult, as the breadth of these features, the relative closeness of the scattering pathways, and resolution limits make delineation difficult. These do suggest a prominent restructuring of the local coordination environment outside of the first shell, associated with the pressure transition. In particular, as the transition is gradual above 35 GPa, it would be expected that further exploration of the RIXS could help to better understand the atomic shuffle associated with the transition.

#### 4. Conclusions

This work has presented the first equation of state results above 100 GPa, high temperature equations of state, and

RIXS and XANES spectroscopic studies of ceria near the phase transition. The application of pressure causes a high pressure structural transition at nearly 35 GPa, with our results indexed using the  $Pnam$  space group, in agreement with previous works [7, 8, 10, 23, 36]. This transition is found to be very sluggish in nature and extends to approximately 73 GPa with a large coexistence region under hydrostatic conditions. Including temperature as a parameter, the phase diagram indicates a discontinuous phase boundary, with regard to the initiation pressure indicating some structural related change between 20 and 200 °C. Further studies are planned to investigate this and extend both pressure and temperature range to determine if a similar occurrence is present for the completion pressures. Comparison between hydrostatic and non-hydrostatic conditions illustrates a substantial change in compressibility, with non-hydrostatic exhibiting a greater bulk modulus. Similarly, the initiation of the transition for the two types of experimental conditions shows a nearly 5 GPa reduction in the transition when non-hydrostatic in pressure.

Pressure increase also shifts of all observed peaks in both the Ce  $L_{III}$ —(RIXS) and  $K$ -edge (XANES) spectra. This was found to initiate at nearly 26 GPa and progress to the limit of these experiments ( $P \approx 33$  GPa). Especially considering the decrease in the initiation pressure associated with non-hydrostatic conditions, it is safe to say that these changes are clearly associated with the phase transition. Beyond just this, the resulting data suggests changes beyond the first coordination shell are ultimately present from comparison of the Fourier transform with the IFEFFIT scattering pathways. This first set of high pressure spectroscopic (RIXS and XANES) studies provides a valuable look at the effects of the high pressure phase transition on ceria. In addition, the high pressure x-ray diffraction results allow a window to help quantify the effects of hydrostaticity on the phase dynamics in ceria, which can likely be extended to cerium metal and other materials. While there is further work required to better understand the relation of the edge energy shift to the high

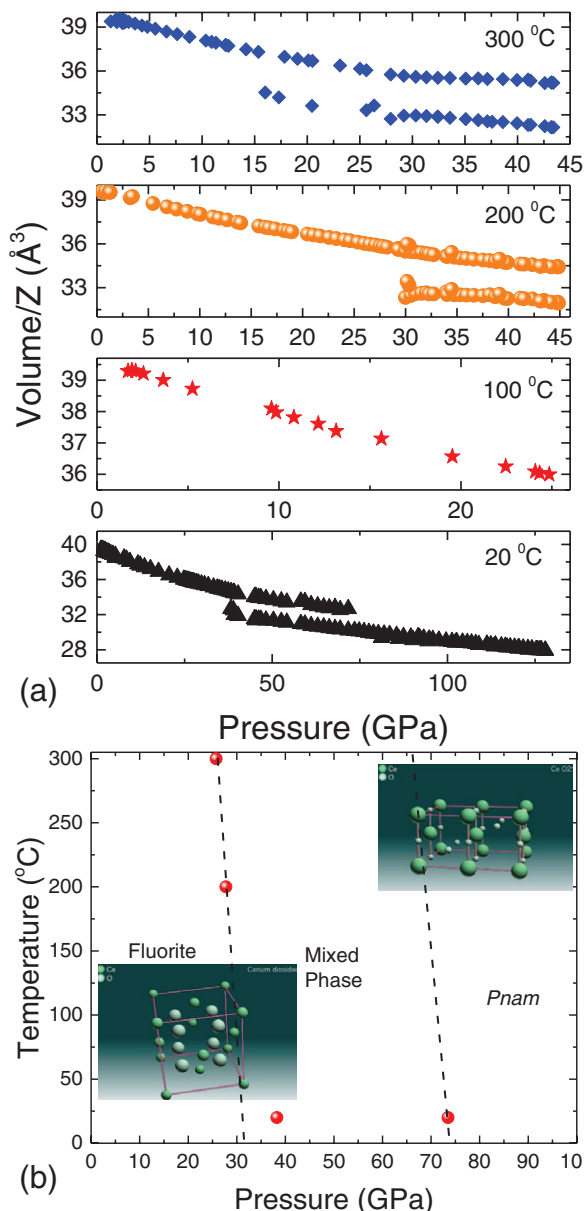


**Figure 4.** Pressures and volumes resulting from the x-ray pattern refinements (a) were extracted and plotted to determine the equations of state associated with the individual isotherms. To help ensure clarity, the individual isotherms have been separated. In each case, the coexistence region between the high pressure and ambient pressure phases is wide ranged and completion is only found for the ambient temperature curve. Initiation and completion pressures for the CeO<sub>2</sub> high pressure phase have been determined and plotted as a function of temperature (b). In this, the ambient pressure points are found to deviate from the high temperature trend. Dashed lines are included in this plot to indicate the high temperature trend for the initiation pressure, with the completion pressure having an identical line projected through the ambient temperature completion point. For the high temperature points, the completion of the transition was not observed up to 45 GPa, suggesting a similar wide coexistence region as with the ambient temperature point. Depictions of the ambient and high pressure phases are inset on the temperature pressure plot.

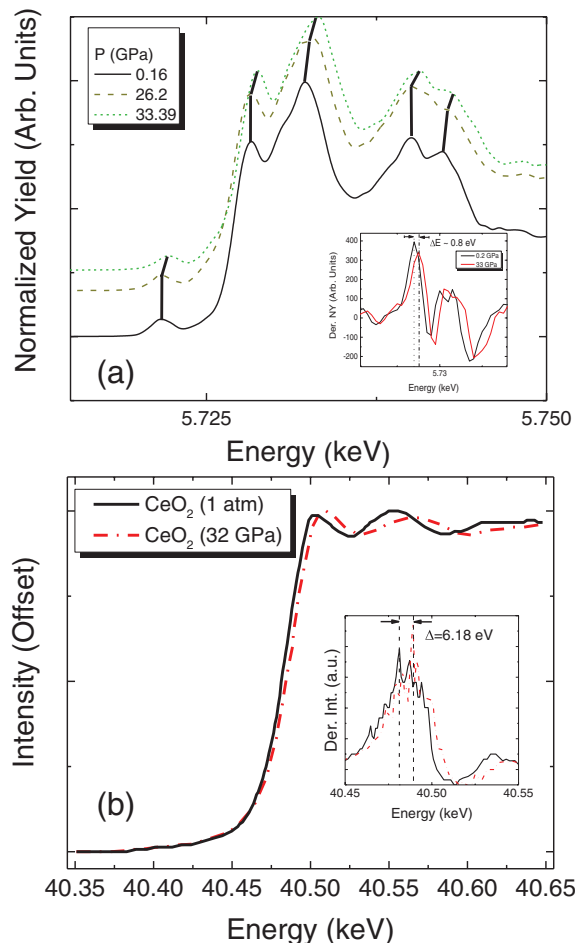


**Figure 5.** Spectroscopic results for CeO<sub>2</sub> with pressure have been obtained for both the  $L_{III}$  (RIXS, (a)) and  $K$  (XANES, (b)) edges. RIXS data shows the pressure progression vertically, with the trends indicated by black lines. XANES spectra of CeO<sub>2</sub> sample at 32 GPa is also shown in comparison with ambient pressure pattern. Insets for both graphs show the derivative curves and indicate the energy shifts of the edge feature.

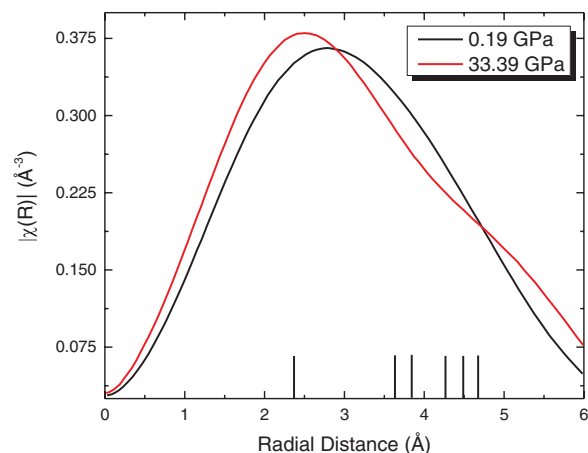


**Figure 6.** Fourier transforms of the RIXS data can be taken to illustrate scattering amplitudes as a function of radial distance. As can be seen, the increase of pressure results in a distinct change, with the centrally located ambient pressure peak splitting with increasing pressure. At the bottom of this figure, the calculated pathways from the IFEFFIT code are illustrated by dark vertical lines. Discussion of these pathways is presented in the text.

pressure structural change, these results present a strong base for extended exploration of actinide oxides and their unique properties.

## Acknowledgments

Los Alamos National Laboratory (LANL) is operated by LANS, LLC for the DOE-NNSA under contract no. DE-AC52-06NA25396. Portions of this work were performed at HPCAT (Sector 16), Advanced Photon Source (APS), Argonne National Laboratory. HPCAT operations are supported by DOE-NNSA under Award No. DE-NA0001974 and DOE-BES under Award No. DE-FG02-99ER45775, with partial instrumentation funding by NSF. Use of the Advanced Photon Source, an Office of Science User Facility operated for the US Department of Energy (DOE) Office of Science by Argonne National Laboratory, was supported by the US DOE under Contract No. DE-AC02-06CH11357. Use of the COMPRES-GSECARS gas loading system was supported by COMPRES under NSF Cooperative Agreement EAR 11-57758 and by GSECARS through NSF grant EAR-1128799 and DOE grant DE-FG02-94ER14466. MKJ gratefully acknowledges the support of the U.S. Department of Energy through the LANL/LDRD Program and the G T Seaborg Institute.

## References

- [1] Yao H 1984 *J. Catalysis* **86** 254–65
- [2] Hay P J, Martin R L, Uddin J and Scuseria G E 2006 *J. Chem. Phys.* **125** 34712
- [3] Trovarelli A 1996 *Catalysis Rev.* **38** 439–520
- [4] Weber W H, Hass K C and McBride J R 1993 *Phys. Rev. B* **48** 178–85
- [5] Van Hung V, Lee J and Masuda-Jindo K 2006 *J. Phys. Chem. Solids* **67** 682–9
- [6] Walkenhorst A, Schmitt M, Adrian H and Petersen K 1994 *Appl. Phys. Lett.* **64** 1871–3
- [7] Duclos S, Vohra Y, Ruoff A, Jayaraman A and Espinosa G 1988 *Phys. Rev. B* **38** 7755–8
- [8] Gerward L, Staun Olsen J, Petit L, Vaitheeswaran G, Kanchana V and Svane A 2005 *J. Alloys Compd.* **400** 56–61
- [9] Kourouklis G A, Jayaraman A and Espinosa G P 1988 *Phys. Rev. B* **37** 4250–3
- [10] Liu L *et al* 2012 *J. Appl. Phys.* **112** 013532
- [11] Errandonea D, Meng Y, Somayazulu M and Häusermann D 2005 *Physica B* **355** 116–25
- [12] Velisavljevic N, Chesnut G N, Stevens L L and Dattelbaum D M 2011 *J. Phys.: Condens. Matter* **23** 125402
- [13] Yashima M, Kobayashi S and Yasui T 2006 *Solid State Ion.* **177** 211–5
- [14] Tracy C L *et al* 2015 *Nat. Commun.* **6** 6133
- [15] Holzapfel W B 2003 *J. Appl. Phys.* **93** 1813
- [16] Dorogokupets P I and Dewaele A 2007 *High Press. Res.* **27** 431–46
- [17] Angel R J 2015 EOSFit
- [18] Materials Data I Jade 2015
- [19] Shen G *et al* 2008 *High Press. Res.* **28** 145–62
- [20] Park C, Popov D, Ikuta D, Lin C, Kenney-Benson C, Rod E, Bommannavar A and Shen G 2015 *Rev. Sci. Instrum.* **86** 072205
- [21] Errandonea D, Muñoz A and Gonzalez-Platas J 2014 *J. Appl. Phys.* **115** 2014–7
- [22] Birch F 1947 *Phys. Rev.* **71** 809
- [23] Gerward L and Olsen J S 1993 *Powder Diffr.* **8** 127
- [24] Piermarini G J J, Block S and Barnett J D D 1973 *J. Appl. Phys.* **44** 5377
- [25] Angel R J, Bujak M, Zhao J, Gatta G D and Jacobsen S D 2007 *J. Appl. Crystallogr.* **40** 26–32
- [26] Zhang J *et al* 2005 *J. Phys. Chem. Solids* **66** 1213–9
- [27] Kaindl G, Schmiester G, Sampathkumaran E V and Wachter P 1988 *Phys. Rev. B* **38** 10174–7
- [28] Sham T, Gordon R and Heald S 2005 *Phys. Rev. B* **72** 035113
- [29] Jo T and Kotani A 1985 *Solid State Commun.* **54** 451–6
- [30] Delley B and Beck H 1985 *J. Magn. Magn. Mater.* **47–8** 269–70
- [31] Bianconi A, Marcelli A, Dexpert H, Karnatak R, Kotani A, Jo T and Petiau J 1987 *Phys. Rev. B* **35** 806–12
- [32] Zhang J, Naka T, Ohara S, Umetsu M and Adschiri T 2006 *Photon Factory Activity Report (Ibaraki: KEK)* <http://pfwww.kek.jp/acr2005pdf/>
- [33] Kotani A, Kvashnina K, Butorin S and Glatzel P 2011 *J. Electron Spectrosc. Relat. Phenom.* **184** 210–5
- [34] Kvashnina K O, Butorin S M and Glatzel P 2011 *J. Anal. At. Spectrom.* **26** 1265
- [35] Ravel B 2006 Demeter, Athena and Artemis
- [36] Liu B, Liu R, Li Q J, Yao M G, Zou B, Cui T, Liu B B and Liu J 2013 *Chin. Phys. C* **37** 098003